Analytical Methods

Accepted Manuscript

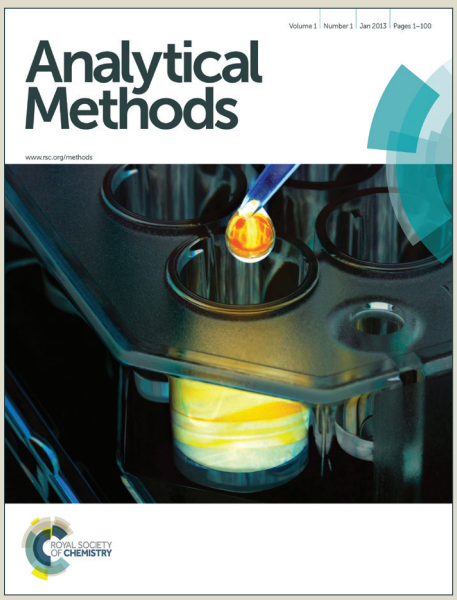

ROYAL SOCIETY OF CHEMISTRY

www.rsc.org/methods

Water-soluble pyridine based colorimetric chemosensor for naked eye detection of silver ion: Design, synthesis, spectral and theoretical investigation

B. Annaraj and M.A. Neelakantan*

Chemistry Research Centre, National Engineering College, K.R.Nagar, Kovilpatti - 628 503, Thoothukudi District, Tamil Nadu, India

Email:maneels@rediffmail.com; drmaneelakantan@gmail.com

Author Information

*Corresponding Author

E-mail: drmaneelakantan@gmail.com, maneelakantan@nec.edu.in

Telephone: +919442505839

Fax.: +914632232749

Abstract

Design and synthesis was performed with the aim of producing water soluble pyridine containing Schiff base as chemosensor. The chemosensor (**L**) was synthesized by reaction between pyridoxal and 2-aminoethanol and comprehensively characterized by elemental analysis, spectroscopic methods (IR, UV−vis, ^{1}H and ^{13}C NMR spectroscopy), ESI mass spectrometry, and by single crystal X-ray crystallography. The designed compound shows excellent specificity and sensitivity (detection limit = 4.18×10^{-6} M) towards Ag^{+} ions over other interfering cations (Na^{+}, K^{+}, Li^{+}, Ca^{2+}, Co^{2+}, Cu^{2+}, Fe^{2+}, Fe^{3+}, Hg^{2+}, Mn^{2+}, Ni^{2+}, $Zn^{2+}$and Pb^{2+}) in aqueous solution. The **L** showed a selective chromogenic behavior towards Ag^{+} ions by changing the color of the solution from light yellow to red, which can be detected with naked eye. Simple and cost effective test kit has been prepared for the detection of silver ion in water samples. The TD-DFT calculations were carried out to understand the sensing mechanism.

Introduction

Sensor is a material that produces detectable signal upon binds selectively with the target analyte[1-5]. Many researchers have focused their research towards the design and synthesize of new sensor materials for wide applications especially for heavy transition metal ion[6-9], because heavy metals play crucial roles in the areas of biological, environmental, and chemical systems[10,11]. Chemosensors bind with the analyte through non-covalent interactions and produce measurable optical signals with immediate response. The important advantage of chemosensor is highly selective, sensitive and reusable [12]. Even though a number of new chemosensors have been reported in recent years, most of them fail to work in aqueous medium. This is only because of their poor solubility in water. The development of water soluble chemosensors for heavy metal ions is a demanding area of research.

A few fluorescent and colorimetric chemosensors have been reported in recent years, which can detect Ag^+ in organic solvent[13-15] or mixed aqueous solution[16,17]. But reports on sensors which allow naked-eye detection of silver ions in aqueous medium are very less [18]. Such sensors allow 'naked-eye' detection of ions without the need to resort to any spectroscopic instrumentation. Ag^+ is extensively used in the electrical, photography, and pharmaceutical industries [19, 20]. These industries are dumping their industry effluents into the nearby aquatic system. Because of the high toxicity of Ag^+ in aquatic organisms, it is important to monitor the Ag^+ level. Moreover, silver is found to inactivate the function of sulphydryl enzymes and started to accumulate in the body [21]. Various instrumentation techniques such as coupled plasma mass spectrometry (ICP-MS) [22] and atomic absorption spectrometry [23] have been currently used to detect the silver ions. Being costly and time-consuming processes, these techniques are not frequently used.

Schiff bases are known for their easy chelation with metal ions. The syntheses of Schiff bases are usually simple and easy. Therefore, Schiff base derivatives having capabilities with optical sensing of metal ions is noteworthy. Herein, we have reported a new Schiff base chemosensor (L) that recognizes the metal ions in aqueous solution. Among the various metal ions examined, the chemosensor **(L)** exhibits a selective

colorimetric response against silver ion. Various spectral (UV-Visible and emission) techniques and Density Functional Theory (DFT) have been used to understand the mechanism through which compound L recognize the silver ion.

Experimental section:

Materials and measurements

Chemicals used in this study were purchased from Sigma Aldrich and used as received. Solvents were procured from the commercial suppliers. The ^{1}H NMR and ^{13}C NMR spectra were recorded in $CDCl_3$ solvent on Bruker-AMX 400 MHz instrument. Electrospray ionization mass spectra (ESI-MS) were obtained from Thermo Finnigan LCQ 6000 advantage max ion trap mass spectrometer. IR spectra on KBr pellets were recorded on a Shimadzu FT IR-8400 spectrometer in the range of 4000–400 cm^{-1}. The absorption spectra were recorded at room temperature using Shimadzu-2450 UV -Visible spectrophotometer. The emission spectra were recorded using Perkin-Elmer LS45 luminescence spectrometer. Single crystal data were collected from Bruker Kappa Apex II single crystal diffractometer and X Shell software was used for solving the structure.

Synthesis of (E)-4-((2-hydroxyethylimino) methyl)-5-(hydroxymethyl)-2-methylpyridin-3-ol (L)

The free pyridoxal was acquired by the dropwise addition of aqueous potassium hydroxide solution (2 N) to pyridoxal hydrochloride (203 mg, 1.0 mmol) in methanol (10 mL) with constant stirring. To this solution was added dropwise 2-aminoethanol (61 mg, 1 mM) in methanol. This reaction mixture was stirred for 1 h at room temperature under nitrogen atmosphere. The volume of reaction mixture was reduced to one third of its original volume and slow evaporation at room temperature yielded large yellow colored crystals which were separated by filtration and washed with ice cold methanol (Scheme S1).

Yield: 150 mg (69%), M.P 132 °C ; Anal. Calc. For $C_{10}H_{14}N_2O_3$: C, 57.13; H, 6.71; N, 13.33. Found C, 57.20; H, 6.69; N, 13.37; ^{1}H NMR ($CDCl_3$, 400 MHz) δ/ppm 2.35 (S, 3H), 3.6 (t, 2H), 3.73 (t, 2H), 4.6 (s,2H), 4.8 (s,1H) 5.4 (s,1H), 7.8 (s, 1H), 8.8 (s, 1H), ^{13}C NMR ($CDCl_3$, 400 MHz) 18.7 (CH_3), 58.3(C-OH), 60.4 (C-OH), 60.7 (N-CH_2),

118.7 (C-C), 132.8 (C=C), 136.7 (C-CH_3), 148.7 (Pyridine C=N), 155.1 (Ar-C-OH), 164.3 (C=$N_{Azomethine}$), ESI-MS m/z $(M + H)^+$: calcd, 211.10; found, 211; IR (cm^{-1}, KBr pellet): 3385 (b, νO–H), 2993–2864 (νC–H), 1617 (νC=N), 1610, 1427, 1404, 1232,1064, 868.

X-ray Diffraction Studies

Single crystal X-ray diffraction experiments were performed on a Bruker Kappa Apex II single crystal diffractometer operating at 50 kV and 0.6 mA using MoKα radiation (λ = 0.71073A˚). Yellow coloured crystal of **L** with dimensions of 0.40 mm × 0.35 mm × 0.30 mm was fixed on the top of a glass fiber and transferred to the diffractometer. The data collected at 293 (2) K is shown in Table S1. The structure was solved by direct methods procedure using SHELXS-97 program [24] and refined by full-matrix least-squares method SHELXL-97 program. All the non-hydrogen atoms were refined using anisotropic atomic displacement parameters and hydrogen atoms bonded to carbon were inserted at calculated positions using a riding model. Hydrogen atoms bonded to oxygen were located from difference map and allowed to refine with temperature factors riding on those of the carrier atoms. The geometrical parameters were obtained using PARST [25] and SHELXL-97.

Metal sensing analysis:

The test solution containing equimolar concentration of L and M (1:1) was prepared by the following procedure. The solution 10 mL of 0.01 M stock solutions of metal salt (Na^+, K^+, Li^+, Ca^{2+}, Co^{2+}, Cu^{2+} , Fe^{2+}, Fe^{3+}, Hg^{2+}, Mn^{2+}, Ni^{2+}, $Zn^{2+}$and Pb^{2+}) were prepared in double distilled water. Stock solution of **L** (1.051 mg, 1 mmol) was prepared in double distilled water for 5 mL. Metal sensing was evaluated by mixing **L** and metal ion to 1:1 molar ratio. The test solutions were prepared by the following procedure. 100 μL of stock solution of **L** was added into the each glass bottles containing 10 μL of individual metal ion stock solution. Then the solution was diluted to 5 mL with water. After mixing the solutions properly, the UV-vis spectra and emission spectra were taken for each sample at room temperature. UV-vis and fluorescence titration were also carried out by keeping the concentration of **L** (20 μM) and varying the silver ion concentration

from 0.5-15 equivalents. Competition experiments were performed in the presence of Ag^+ mixed with various metal ions in the ratio of 1:1:2 of L : Ag^+ : M.

Job plot analysis:

The **L** (1.051 mg, 1 mmol) was dissolved in water (5 mL). 20, 40, 60, 80, 100, 120, 140, 160, 180 μL of the solution was taken from the stock solution and transferred to a vial. To make a total volume of 200 μL in the vial, the remaining volume (180, 160, 140, 120, 100, 80, 60, 40, 20 μL of the Ag^+ solution) was taken from the stock solution of Ag^+ (0.34 mg, 1 mmol). Then the solutions were diluted to 2 mL with water. The solutions were shaken well before recording the UV-Visible spectra at room temperature. The Job's plot was constructed by using change in absorbance for free metal and ligand bound metal (D-D') vs. mole fraction of metal ion. The binding constant (K_a) was estimated using Benesi–Hildebrand plot, involving plot of the inverse of metal ion concentration against the inverse of changes in its absorbance ($1/(A\text{-}A_o)$ vs. $1/[Ag^+]$). The following equation was used to calculate the binding constant [26],

$$\frac{1}{(A - A_0)} = \frac{1}{K_a(A_{min} - A_0)[Ag^+]} + \frac{1}{(A_{min} - A_0)}$$

Results and Discussion

Synthesis and general aspects

The **L** was synthesized by the condensation between pyridoxal and 2-aminoethanol. **L** is soluble in water and other organic solvents (methanol, ethanol, acetonitrile, dimethyl sulphoxide and dimethyl formamide). The structure of **L** was characterized by IR, UV-vis, NMR and ESI-Mass techniques. The formation of Schiff base is confirmed by the IR band observed at 1617 cm^{-1} [ν(C=N)] and 1232 cm^{-1} [ν(phen C-O)] [27]. It is further confirmed by ^1H and ^{13}C NMR (Fig. S1 & S2) and ESI-Mass spectra (Fig. S3). In aqueous solution, UV-vis spectrum of **L** shows three distinct bands at 220, 280, 330 nm correspond to π-π* and n-π* transitions.

Crystal Structure of L

Crystallographic data and refinement details for the structural analysis of **L** are given in (Table S1). Fig. 1 shows the atom numbering scheme and the thermal ellipsoid plot for the **L** drawn at 50% probability level using the program ORTEP [28]. The compound crystallized into a monoclinic crystal lattice system with the space group of C2/C. The selected bond lengths and angles are given in Table S2. The molecule is highly stabilized by inter and intra molecular hydrogen bonding. The unit cell packing diagram of **L** viewed along the C axis is given in Fig. S4. The presence of ortho hydroxyl group in Schiff bases favours the existence of intramolecular hydrogen bonding and also the tautomerism accounting for the formation of either phenol–imine (O H···N) or keto-amine (O···H N) tautomers [29]. The molecular conformation of **L** is stabilized by intramolecular O1-H···N1 hydrogen bond (2.5 Å), generating S(6) motif. The N(1)–C(8) bond length is 1.26 Å, which is smaller than the reported bond length for a single C–N bond (1.437 Å) [30]. But, this bond length is very close to the mean bond length reported for a C=N double bond (1.289 Å) [31]. This results reveals the existence of double bond between N(1)–C(8). The bond distance for O(1)-C(5), O(2)-C(1), O(3)-C(10) are 1.33, 1.40, 1.41 Å respectively. The bond distance of C(5)-O(1) in **L** is consistent with the C–O single bonding. The C–O and C=N bond distance indicates the presence of phenol–imine form of the molecule in the crystalline state. The molecular packing of **L** is also stabilized by O2-H…O3 and O3-H…N2 intermolecular hydrogen bonding.

Evaluation of metal ion sensor

Evaluation of metal sensing capacity of **L** has been evaluated by UV-Visible and fluorescence techniques with different metal ions *i.e,* Na^{+}, K^{+}, Li^{+}, Ca^{2+}, Ag^{+}, Co^{2+}, Cu^{2+} , Fe^{2+},Fe^{3+}, Hg^{2+}, Mn^{2+}, Ni^{2+}, $Zn^{2+}$and Pb^{2+} in complete aqueous medium. The probe **L** showed λ_{max} at 280 nm and 330 nm. Among the various metal ions tested, **L** responded selectively to Ag^{+} ion by producing the colour change from yellow to red (Fig. 2). This colourimetric change occurred may be due to the formation of new λ_{max} values at 359 and 517 nm in UV-Visible spectra of **L** (Fig. 3). This observation indicates that **L** has a pronounced selectivity for Ag^{+} over the other metal cations screened herein. Furthermore the addition of other biologically important metal ions directed no apparent change in the ground state behaviour of **L**.

In order to ensure the selectivity for the analyte (Ag^+) over the other metal ions, competition experiment were carried out by adding the Ag^+ into the solution of **L** in the presence of other metal ions. The UV-visible and fluorescence titrations were carried out for **L** against Ag^+ in the presence of two equivalents of Na^+, K^+, Li^+, Ca^{2+}, Co^{2+}, Cu^{2+} , Fe^{2+}, Fe^{3+}, Hg^{2+}, Mn^{2+}, Ni^{2+}, Zn^{2+} and Pb^{2+} ions. None of these metal ions significantly affect the absorption and fluorescence intensity of L–Ag^+ system. The result of this study reveals that sensing capacity of **L** did not affect by the common co-existing metal ions. Also, the results indicate that Ag^+ is not being replaced by other metal ions from the binding core of **L**.

In the emission spectra, when excited at 359 nm the probe **L** shows a low intensity emission band at 525 nm. Upon addition of different metal ions, the **L** exhibits a remarkable fluorescence enhancement only with Ag^+ rather than with other metal ions (Fig. 4).

The absorption and fluorescence intensity of **L** increases with increasing the concentration of silver ion (Fig. S5 & 5) and it is not suppressed while adding the competitive metal ions (Fig. 6). The increase in emission intensity is due to the formation of the L–Ag^+ complex causing the inhibition of the C=N isomerization [32] and chelation-enhanced fluorescence effect. The chelation of Ag^+ with **L** effectively increases the coplanarity of **L** and decreases the loss of energy through non-radiative transition that lead to fluorescence enhancement [32]. Hence, the azomethine nitrogen, phenolic -OH and aliphatic -OH play an important role in the efficient binding of **L** with Ag^+. The results of job plot analysis and ESI-mass spectrum revealed the formation of 1:1 complex (Fig. S6 & S7). Detection limit was measured by the formula 3σ/slope and found to be 4.18×10^{-6} M with RSD of 2.2% (Fig. S8). The binding constant of **L** with Ag^+ was calculated as 4.95×10^4 M^{-1} on the basis of Benesi–Hildebrand plot (Fig. S9). These results are showing the better sensing and binding affinity of **L** with Ag^+.

Reversibility is a prerequisite in developing novel chemosensors for practical application. The reversibility of the recognition process of probe **L** was performed by adding an Ag^+ bonding agent, Na_2EDTA. The addition of EDTA to a mixture of probe **L**

and Ag^+ resulted in quenching of the fluorescent intensity at 525 nm, indicating the regeneration of the free probe **L**.

^1H NMR spectroscopy was employed to get information about the binding of silver ion with **L**. ^1H NMR spectrum of **L** with one equivalent of $AgNO_3$ was recorded in D_2O. Shielding effect is observed than the original spectrum of L (Fig. S10). A little deshield shift experienced by the protons; H_g, H_b and H_c rather than other protons, illustrate the imprisonment of Ag^+ into the O_2N cap of **L**. It is further supported by the theoretical calculations which are given in the supporting information.

The pH sensitivity of the probe was tested by recording the UV-Visible spectra at different pH values. **L** shows two different UV-Visible spectra at lower and higher pH values of the solution. This clearly indicates that L undergoes protonation and deprotonation process with respect to pH. At lower pH, **L** shows four distinct absorption bands at 203, 253, 288, 318 nm correspond to the protonated form of L (Fig. S11). At higher pH, the band at 318 nm started to disappear and a new absorption band appears at 393 nm corresponds to the deprotonated form of **L**. The effect of pH on sensing capacity of **L** towards Ag^+ was examined. Over the pH range tested, the absorption spectra of L-Ag showed strong pH dependence. The compound L showed a meaningful response to Ag^+ ion in the pH range of 4.5-9 which are relevant to physiological pH.

In order to study the practical application of **L**, we have prepared a test kit made by the filter paper. The filter paper is immersed in the aqueous solution of **L** (20 μM). After dried in air, the filter paper becomes yellow in colour. The filter paper changes its colour within a minute from yellow to dark brown when it was dipped in the aqueous solution of Ag^+ (20 μM) ion (Fig. 7). So this test kit would be simple and useful to detect the silver ion in complete aqueous medium.

To assess the practical applicability of L to real water samples, analysis was carried out for the detection of silver ion in drinking water, bore well water and tap water. Insoluble materials present in the samples were removed by filtration. Initial silver ion concentration of the samples was estimated by AAS. Then 40 μM concentration of silver ion was added in each sample and it was estimated by test kit followed by absorption spectral data. The observed results are given in Table S3. The observed results show the

practical applicability of **L** for the detection of Ag^+ in real water samples without any interference from other metal ions.

Conclusions

We report the design and synthesis of a water-soluble pyridine based chemosensor for the naked eye detection of silver ion in complete aqueous medium (pH 7.3). The sensor is selective for Ag^+ detection in aqueous solution containing different metal ions. The detection limit of Ag^+ ion is as low as 4.18×10^{-6} M in aqueous solution without any interference from other metal ions. The studies revealed that the sensor makes interaction with silver ion in the ratio of 1:1. Computational calculations support the binding mode proposed between compound **L** and Ag^+ ion and the fluorescence behaviors. The practical applicability of the probe has been tested with different real samples.

Supplementary Information

CCDC 1010922 contains the supplementary crystallographic data for this paper. These data can be obtained free of charge from the Cambridge Crystallographic Data Centre via. http://www.ccdc.cam.ac.uk/cgibin/catreq.cgi. Computational calculation procedures, discussion, additional figures, tables and references are given.

Acknowledgement

M.A.N gratefully acknowledges the financial support from Department of Science and Technology (DST), New Delhi, India (SR/S1/IC-08/2010). B.A thanks DST for the fellowship. CSIR, New Delhi is acknowledged for partial financial support (01(2736)/13/EMR-II). STIC, Cochin is acknowledged for SCXRD analysis.

References:

1. J.P. Desvergne, A.W. Czarnik (Eds.), *Chemosensors for Ion and Molecule Recognition*, Kluwer, The Netherlands, 1997.

2. H. L. Li, J. L. Fan, J. J. Du, K. X. Guo, S. G. Sun, X. J. Liu and X. J. Peng, *Chem. Commun.*, 2010, **46**, 1079–1081.

3. Y. Yang, C. Gao, B. Li, L. Xu, L. Duan, *Sensors and Actuators B: Chemical*, 2014, **199**, 121-126.
4. J. Wang, W. Lin, L. Yuan, J. Song and W. Gao, *Chem. Commun.,* 2011, **47**, 12506–12508.
5. H. N. Kim, W. X. Ren, J. S. Kim, J.Yoon, *Chem. Soc. Rev.,* 2012,**41**, 3210-3244
6. M. Beija, C.A.M. Afonso, J.M.G. Martinho, *Chem. Soc. Rev.* 2009, **38**, 2410-2433
7. E.M. Nolan, S.J. Lippard, *Chem. Rev.* 2008, **108,** 3443-3480.
8. A. K. Mandal, M. Suresh, E. Suresh, S. K. Mishra, S. Mishra, A. Das, *Sens. Actuators B,,* 2010, **145**, 32–38.
9. S. Pal, N. Chatterjee, P. K. Bharadwaj, *RSC Adv.,* 2014,**4**, 26585-26620
10. E. Merian (Ed.), *Metals and their Compounds in the Environment: Occurrence, Analysis and Biological Relevance*, VCH, New York, 1991.
11. M.H. Keefe, K.H. Benkstein, J.T. Hupp, *Coord. Chem. Rev.* 2000, **205**, 201-228.
12. T. Ueno, T. Nagano, *Nat. Methods,* 2011, **8**, 642-645.
13. V. Tharmaraj, S. Devi, K. Pitchumani, *Analyst*, 2012, **137**, 5320-5324
14. C. Li, X.F. Kong, Y.F. Li, C. X. Zou, D. Liu, W.G. Zhu, *Dyes Pigm.,* 2013 ,**99**, 903-907
15. F. Wang, R. Nandhakumar, J. H. Moon, K.M. Kim, J. Y. Lee, J. Yoon, *Inorg. Chem.* 2011, 50, 2240–2245
16. K.M. K.Swamy, H. N. Kim, J. H.Soh, Y. Kim, S.-J. Kim, J. Yoon, *Chem. Commun*. 2009, 1234-1236.
17. A. Chatterjee, M. Santra, N. Won, S. Kim, J. K. Kim, S. B. Kim, K.H. Ahn, *J. Am. Chem. Soc.* 2009, **131**, 2040-2041.
18. M.Hu, J.J.fan, J.Cao, K.Song,H.Zhang, S.Sun, X.Peng, *Analyst*, 2012, **137**,2107-2111.
19. J. L. Barriada, A. D. Tappin, E. H. Evans, E. P. Achterberg, *TrAC, Trends Anal. Chem.* 2007, **26**, 809-817.
20. H. T. Ratte, *Environ. Toxicol. Chem.* 1999, **18**, 89-108.
21. X. Zhang, Z. Han, Z. Fang, G. Shen, R. Yu, *Anal. Chim. Acta*, 2006, **562**, 210-215.

22. D. Karunasagar, J. Arunachalam, Gangadharan, S. *J. Anal. At. Spectrom.* 1998, **13**, 679-682.

23. Y. Li, C. Chen, B. Li, J. Sun, J. Wang, Y. Gao, Y. Zhao, Z. Chai, *J. Anal. At. Spectrom.* 2006, **21**, 94-96.

24. G.M. Sheldrick, SHELXS-97 and SHELXL-97, Program for the Solution of Crystal Structures, University of Gottingen, Germany, 1997.

25. M. Nardelli, *J. Appl. Cryst*. 1995, **28**, 659.

26. K. A. Connors, *Binding Constants*; Wiley, New York, 1987, pp. 147-187

27. B. Stuart, *Infrared Spectroscopy: Fundamentals and Applications*, 1st Edition, John Wiley & Sons, Ltd , 2004

28. Johnson, C.K., Guerdon, J.F., Richard, P., Whitlow, S., and Hall, S.R. 1972. ORTEP. The X-RAY system of Crystallographic Programs. TR-192, p 283

29. V. Selvarani, B. Annaraj, M.A. Neelakantan, S. Sundaramoorthy, D. Velmurugan, *Spectrochim. Acta A* , 2012, **91** 329– 337

30. D. Ray and P. K. Bharadwaj, *Inorg. Chem.,* 2008, **47**, 2252-2254

31. L. Xue, Q. Liu and H. Jiang, *Org. Lett.,* 2009, **11**, 3454 -3457

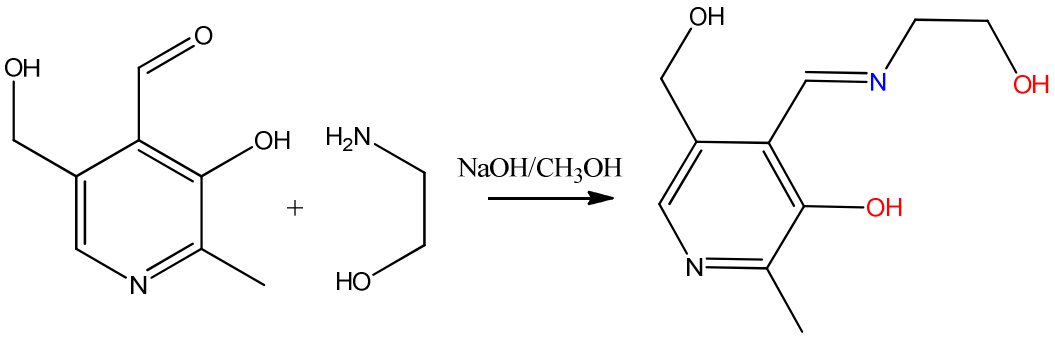

Scheme 1 Synthetic scheme of **L**

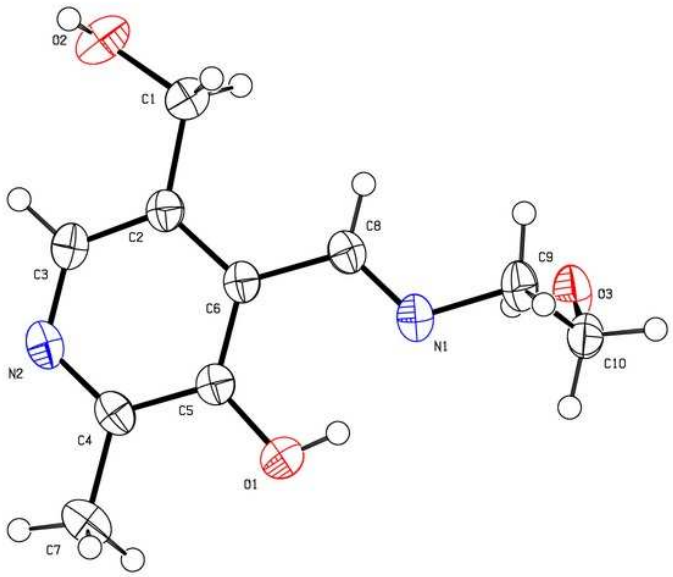

Fig. 1 ORTEP Diagram of **L**

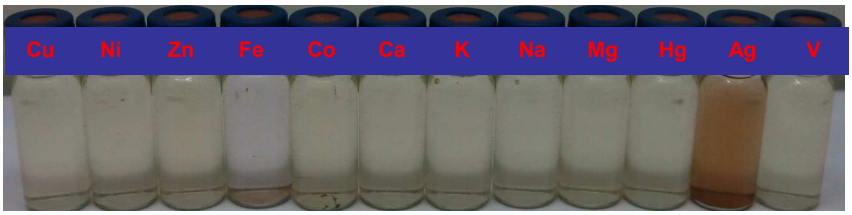

Fig. 2 Photographic image of **L** (20 μM) in the presence of different metal ions

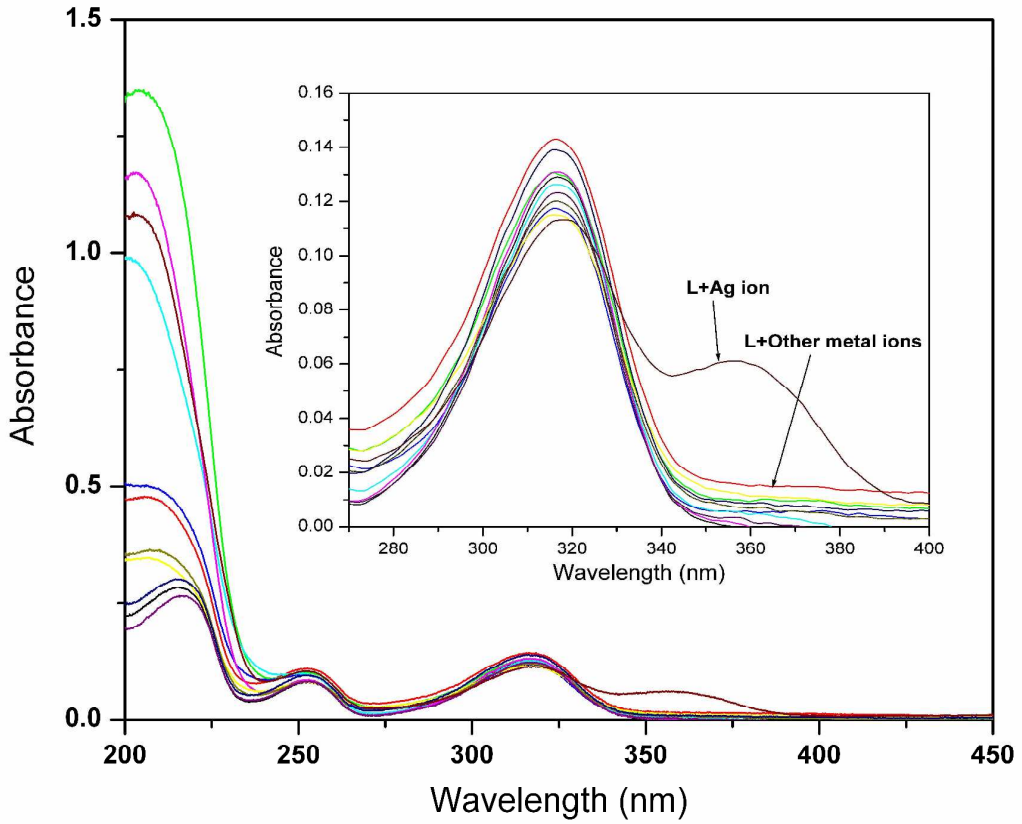

Fig. 3 Electronic absorption spectra of **L** (20 μM) in presence of different metal ions (20 μM) Cu, VO, Zn, Ni, Co, Fe, Ca, K, Na, Ag

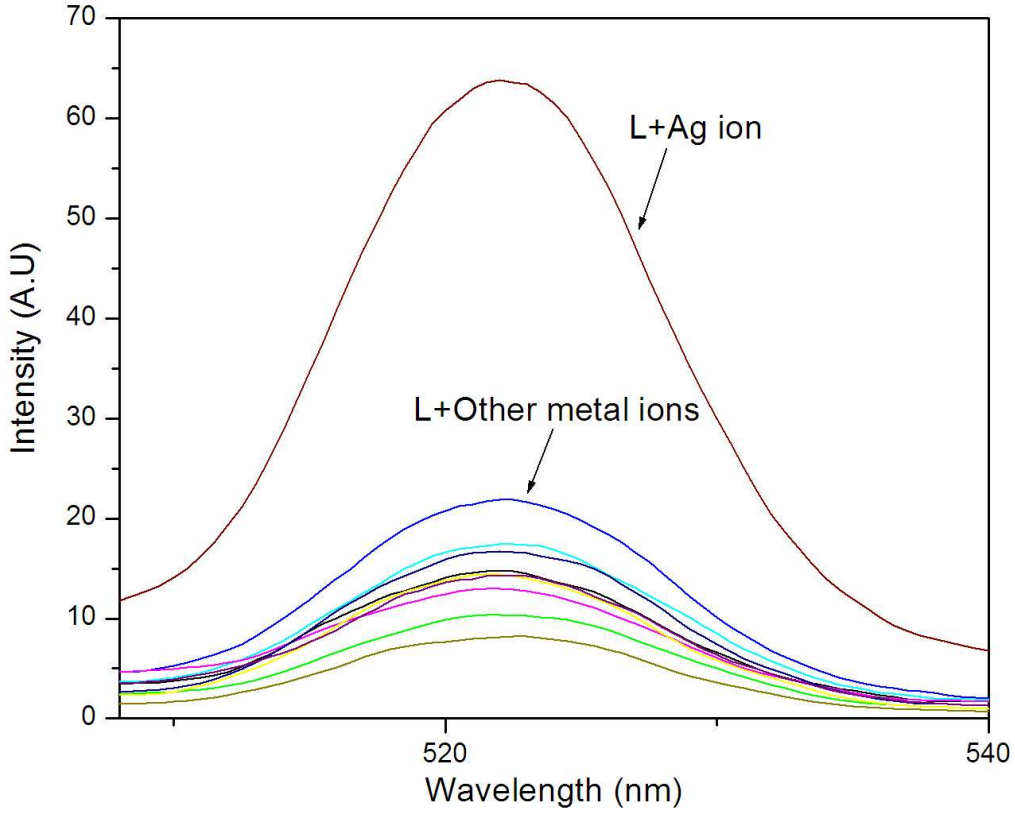

Fig. 4 Emission spectra of **L** (20 μM) in presence of different metal ions (20 μM) Cu, VO, Zn, Ni, Co, Fe, Ca, K, Na, Ag (λ_{ex}=359 nm)

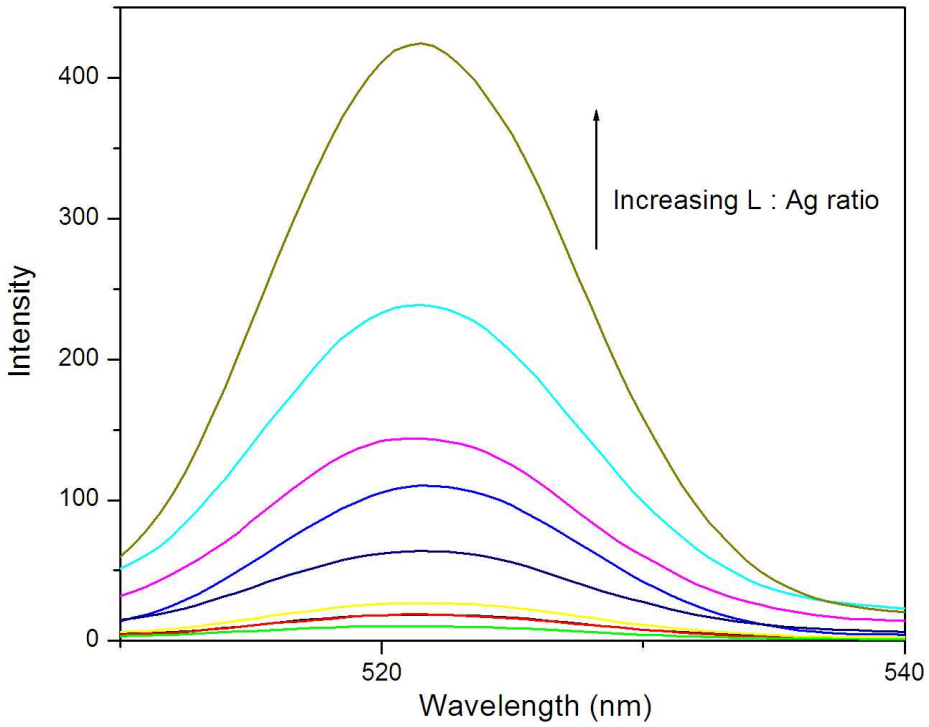

Fig. 5 Emission spectra of **L** (20 μM) in presence of different equivalents (0.5-15 eq) of Ag^{+} ions

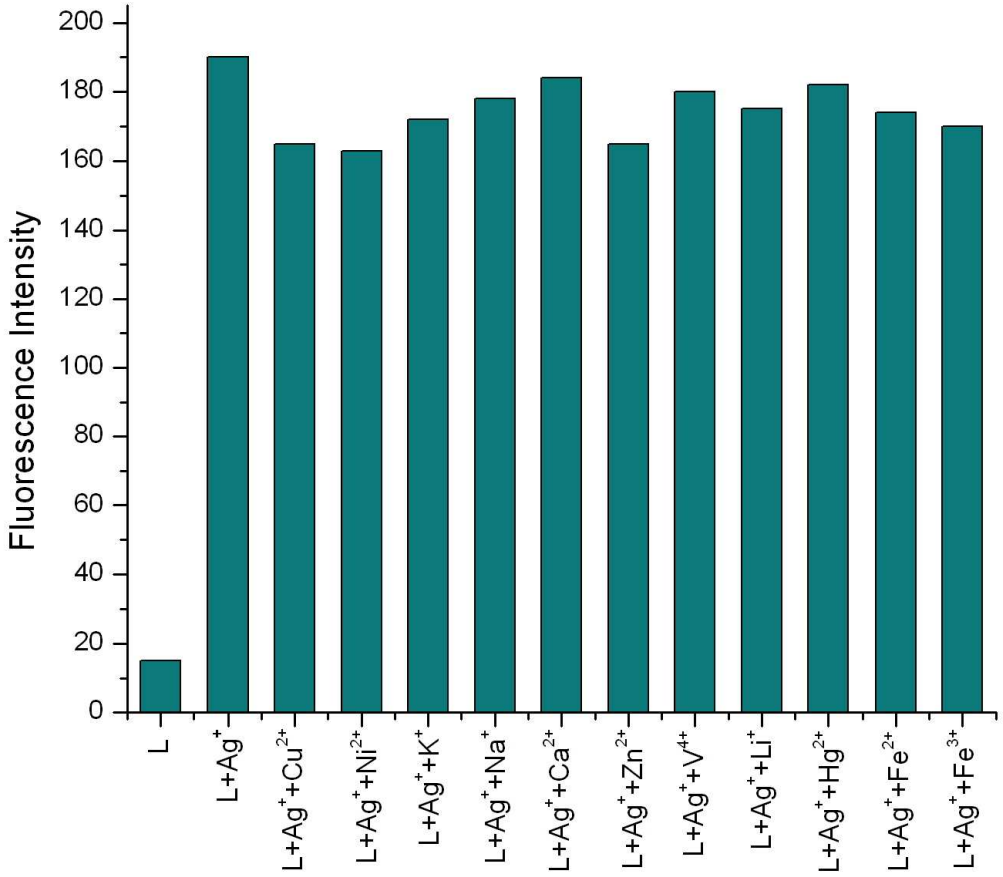

Fig. 6 Fluorescence intensity at 525 nm of L+Ag in presence of competitive metal ions (λ_{ex}=359 nm).

Fig. 7 Photographs of the filter paper coated with L used for the detection of Ag^{+}. (a) Filter paper coated with L (20 μM), (b) Probe **L** test kit immersed in Ag^{+} solution.